3A.1   **SENSITIVITY OF CONVECTIVE INITIATION AND SUBSEQUENT
CONVECTION BASED ON ENVIRONMENTAL PARAMETERS USING 500M
RESOLUTION WRF ARW**

Justin T. Schultz* and Christopher J. Anderson
Iowa State University, Ames, Iowa

1. INTRODUCTION

Convective initiation (hereafter denoted as CI) is defined as the development of cumulus convection into sustained cumulonimbus clouds resulting in deep, moist convection (Markowski et al. 2006). CI is a particularly difficult forecasting and modeling issue because the most minute changes in atmospheric conditions could either hinder or develop and sustain convection. Understanding when and where CI occurs, and the mechanisms that cause CI, is vital to forecasters for many reasons, particularly in warning the public of imminent severe weather and correctly forecasting precipitation [e.g., quantitative precipitation forecasts (QPFs)].

Clearly, thoroughly understanding the environmental conditions and mechanisms for CI are crucial to solving the issue of CI forecasting. However, forecasting for CI is not easy. Sometimes, it is relatively easy to spot the location of CI due to the presence of a very predominant frontal boundary, such as a dryline or a cold front, where convergence is highest (Byers and Braham 1949). However, it has been shown that more subtle CI mechanisms can give the environment just enough sufficient forcing to break the capping inversion and assist thermals in reaching the level of free convection (LFC) to initiate deep, moist convection. Unfortunately, these types of forcing mechanisms are more difficult to spot by visible satellite imagery, Doppler radar, or even mesonet plots due to how small these mechanisms are relative to other CI mechanisms.

The main focus of this study will be to diagnose the sensitivity of CI to perturbations in the environmental parameters that affect stability, such as changes in the temperature and moisture profiles. We will also observe and diagnose other environmental perturbations using high-resolution tests on the CI mechanisms and observing their response to these parameters. The goals of this study are to: 1) test Markowski et al. (2006) hypotheses that the lack of moisture upwelling contributed to the lack of convection that occurred during a case from the International H_2O Project (IHOP; Weckwerth *et al.* 2004), and 2) diagnose the sensitivity of each CI mechanism based on perturbations in the environment, including potential temperature and water vapor mixing ratio. The authors determined that these two parameters would be the most important parameters to test since the development of deep, moist convection is highly dependent on the stability profile and the amount of moisture contained in the

_____

* *Corresponding author address:* Justin T. Schultz, 3018 Agronomy Hall, Iowa State University, Ames, IA 50010; e-mail: jsch78@iastate.edu.

environment. Sensitivity is based on the change in the CI location and timing, and the development of subsequent convection based on the CI mechanisms. For example, one of the questions that will be answered is: will an increase in potential temperature help or hinder CI development temporally?

This is a case study of a particularly active severe weather event that occurred during IHOP on 12 June 2002, which has been the subject of much research in the past (Markowski et al. 2006; Weckwerth et al. 2008; Liu and Xue 2008). The reason this case is of particular interest is that CI occurred outside of the intensive observation region (IOR) for the IHOP field project. There were numerous CI mechanisms that were present that day including: a dryline, mesoscale low pressure center (mesolow), an outflow boundary left over from previous convection, the intersection of the said outflow boundary and dryline, internal gravity waves (IGWs) and horizontal convective rolls (HCRs; Weckwerth et al. 1997). Weckwerth et al. (2008) documented the deployment and monitoring operations for this case, and mentioned that it was thought that CI would occur near the mesolow in the Oklahoma Panhandle region, but CI actually occurred ~40 km to the east of the IOR (Liu and Xue, 2008).

Obviously, it is very difficult to determine when and where CI will occur simply due to the numerous CI mechanisms in the region for this case. However, two CI mechanisms played the largest roles in initiating convection on 12 June: HCRs and the outflow boundary. Weckwerth *et al.* (2008) showed that there was evidence of roll-like circulations, which were determined to be the HCR circulation. However, even though CI occurred in this vicinity, the environment was more unstable along the outflow boundary, which extended from the eastern section of the Oklahoma Panhandle, east to north-central Oklahoma, and southeast to east-central Oklahoma. It was shown that values of convective available potential energy (CAPE) along the outflow boundary were 5000 J/kg (Wilson and Roberts 2006). Markowski *et al.* (2006) had hypothesized that the development of convection did not occur along the outflow boundary due to a lack of moisture upwelling and a lack of substantial moisture being moved by mesoscale circulations. This hypothesis will be tested by initiating a cold pool ahead of the outflow boundary to determine if CI occurs along the outflow boundary, in the WRF ARW model simulation.

2. METHODOLOGY

It is known that CI and subsequent convection are dependent on environmental conditions (Wilhelmson

and Chen 1982). To test the sensitivity of CI and subsequent convection to the environment that the CI mechanisms dwelled in, we simulated this event using the Weather Research and Forecasting (WRF; Skamarock *et al.* 2001) Advanced Research WRF (ARW) model. This simulation, with no perturbations applied to the environment, became our control simulation, but this event is difficult to be able to simulate accurately since it has been shown that synoptic- and convective-scale CI mechanisms have been found to be present in the observed and the simulated data. Convective-scale phenomena will not be resolved by a model well enough if the model is not of sufficiently fine grid spacing. For example, it is rather difficult for a model to accurately simulate turbulence that occurs on a 10s-of-meters scale if the model resolution is two orders of magnitudes larger. After we obtained data from the control run, we then created a domain to perturb potential temperature and water vapor mixing ratio.

Potential temperature (θ) was increased and decreased logarithmically with height throughout the depth of the boundary layer. We had to change θ using this method since the model simulation repeatedly crashed due to numerical instability by the temperature profiles (e.g. temperatures will make a sharp increase or decrease if we perturbed the temperature by a set amount). On the other hand, water vapor mixing ratio was perturbed by a set amount, which did not cause numerical instability; it was perturbed by ±2 g/kg. These parameters were perturbed through the depth of the boundary layer, which extended up to ~1000 meters AGL ($\gtrsim 900$ mb).

a. Diagnosing the occurrence of CI

In the model simulation, we added an additional section of code that computed the lifted condensation level (LCL; height in meters). We can also compute how high each model level is to determine exactly how high AGL do cumulus clouds develop. From this, we can determine exactly when cumulus clouds in the model reach the LCL, hence initiating deep moist convection. By using the LCL height, we can estimate the CI timing by determining when cumulus clouds develop above 1000 meters.

b. Specifications of the WRF ARW model

We used WRF ARW v.3.1.1 to simulate the CI timing and location, the parameter perturbations, and the cold pool generation. The model was initialized at 2000 UTC and run to 2300 UTC. The domain was centered over the state of Oklahoma, with special attention focused in the northwestern section of Oklahoma, since that is where the observed area of CI occurred. An output file was set to be generated every five minutes of the simulation. For the parameter perturbation simulation, we ran WRF at 2 km grid spacing, with a 400 × 400 grid domain. The model time step was set at 5 seconds. Table 1 shows the parameterization schemes used for the 2 km simulation,

and Figure 1 shows the 2 km grid domain. Plots for this project will be made using the National Oceanic and Atmospheric Administration's (NOAAs) Pacific Marine Environmental Laboratory (PMEL) FERRET software (v.6.62).

Physics	Parameterization Scheme
Microphysics	WRF Double-Moment 6-class scheme
Longwave Radiation	Rapid Radiative Transfer Model
Shortwave Radiation	Dudhia
Surface Layer	Eta similarity
Land Surface	RUC Land Surface Model
Planetary Boundary Layer	MYJ
Cumulus	Off

Table 1: Overview of parameterization schemes used to perturb the environmental parameters.

It is hypothesized that an increase in the potential temperature and the water vapor mixing ratio would make CI occur sooner, and vice versa for a decrease in potential temperature and the water vapor mixing ratio.
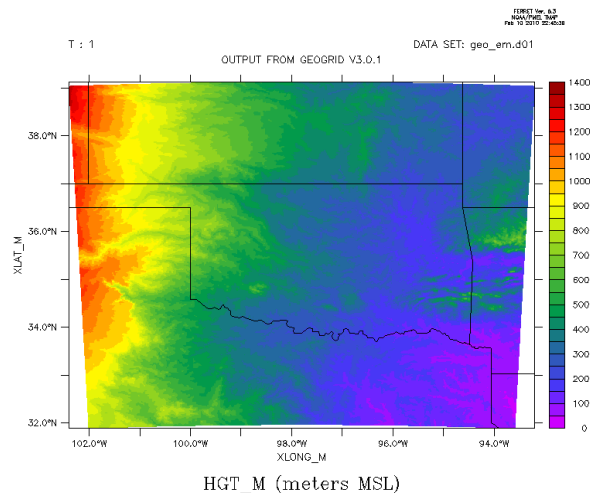

Figure 1: Two kilometer simulation grid domain; used for parameter perturbation simulations. Height (HGT_M) is plotted for reference.

c. Overview of mesoscale conditions on 12 June 2002

A mesoscale low pressure center developed over the Oklahoma Panhandle at ~1200 UTC. An east-west boundary was located along the Oklahoma-Kansas border due to an outflow boundary from the previous evening's mesoscale convective systems (MCSs). At 1800 UTC, the east-west outflow boundary propagated northward, which ushered warm southerly flow on the south side of the boundary. This might have been due to the influence of the mesoscale low pressure center over the Oklahoma Panhandle, since the counter-

clockwise rotation around the mesolow would force air to move north on the right hand side of the mesolow. Intersecting the outflow boundary in northwest Oklahoma was a dryline, which was propagating towards the east. Ahead of the outflow boundary, located in south central Kansas, are some IGWs, which could have helped to focus convective initiation. Finally, it was found that there were HCRs in the vicinity of where CI actually occurred for this event, which suggests that the HCRs helped focus CI (Weckwerth *et al.* 2008).

In previous literature, it has been shown that outflow boundaries assisted in generating internal gravity waves themselves due to the vertical displacement of air in a stably stratified environment (Weckwerth and Wakimoto 1992). However, it is important to note that these internal gravity waves observed in Weckwerth and Wakimoto (1992) were shown to be oriented parallel along the outflow boundary, which gives proof that the outflow boundary assisted in generating IGWs. However, for the 12 June 2002 case the IGWs were oriented nearly perpendicular to the outflow boundary, suggesting that these IGWs were not generated due to the outflow boundary. Thus, these IGWs will be considered an independent CI mechanism for this study.

d. Background information on CI mechanisms

This section contains background information on the CI mechanisms in place for this case study.

1) Horizontal Convective Rolls (HCRs)

HCRs have been studied in literature since the 1960s (i.e., Faller 1965; Lilly 1966). They are defined as counter rotating horizontally oriented rotors that have both an ascending and descending branch to each roll, and they operate as a mesoscale circulation. It has been shown that HCRs require a combination of surface-layer heat flux and wind shear to exist, and the orientation of the roll axes are usually along the mean convective boundary layer (CBL) wind (Weckwerth *et al.* 1997). The depth of HCRs equals that of the boundary layer, and the ratio of lateral to vertical dimensions for a roll pair is roughly 3:1. (Stull 1988).

2) Internal Gravity Waves (IGWs)

IGWs are waves in the atmosphere that are generated by the interaction of a lifting (buoyancy) force and a restoring force (gravity). The result of neither force dominating over the other generates an undulating wave pattern to develop. For this CI case, Weckwerth *et al.* (2008) believed that the IGWs may have helped to

modulate the CBL moisture field. However, in the 2 km simulation, the WRF ARW model did not appear to have successfully resolved the IGWs since there was not any evidence of a wave-like structure in south central Kansas where the IGWs were found in the observed dataset.

3) Drylines

Drylines are considered a synoptic scale boundary which, unlike warm and cold fronts that separate air masses of different temperatures, separates air masses of different moisture content. They commonly form over the southern Great Plains and have been found as far north as the Dakotas (Schaefer 1986). Drylines are known to spawn severe local storms quite often, and it is not surprising that forecasting CI along a dryline is often difficult due to the three-dimensional nature of the dryline structure not being well understood (Atkins *et al.* 1998). A three-dimensional numerical model study showed that CI is typically concentrated along the dryline where sufficient moisture convergence occurs, which acts to destabilize the environment, making it more conducive of CI (Ziegler *et al.* 1997).

4) Outflow boundaries

Outflow boundaries (also known as *gust fronts*) are pools of cool air that are caused by evaporative cooling within a deep moist convective cloud. Once this pocket of cool air reaches the ground, this pool of dense air spreads out, which creates the outflow boundary, which propagates away from the parent storm. The main reason why convection can develop along an outflow boundary is because the gust front is capable of undercutting and forcing warm air upward, due to the gust front's negative buoyancy. Outflows have been known to work in conjunction with Kelvin-Helmholtz waves and internal gravity waves to help initiate convection in specific locations (Weckwerth and Wakimoto 1992).

Before we discuss the results of the simulations, we would like to briefly discuss the circumstances of the observed CI dataset for 12 June 2002.

It was determined that CI occurred at ~2100 UTC on 12 June 2002, near Freedom, OK from visible satellite archives (visible satellite images courtesy of http://www.mmm.ucar.edu/imagearchive/). Convection developed along the dryline and outflow boundary immediately following the initial CI, which occurred ahead of the dryline and behind the outflow boundary. It was first thought that the dryline was the primary CI mechanism for this case (Wilson and Roberts 2006).

However, upon further inspection by Weckwerth *et al.* (2008), it was determined that HCRs helped to focus convection for this case, making it the primary CI mechanism. The HCRs were evident in both the cloud streets observed in satellite imagery and radar composite fields (Weckwerth *et al.* 2008), which gave the evidence to suggest that HCRs were present in the vicinity of CI. The rolls were oriented along the CBL winds and were present within the CBL itself east of the dryline and mesolow locations. Figure 2 shows a synopsis of where each boundary was located just prior to 2100 UTC.
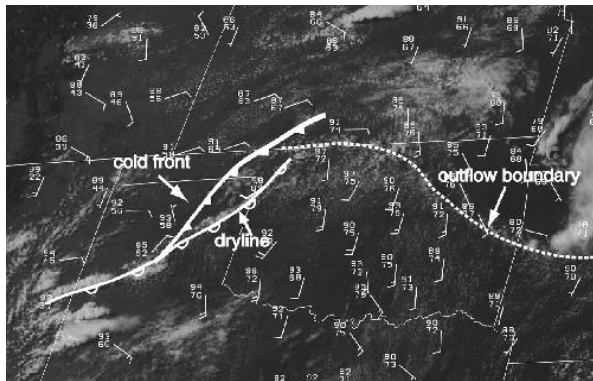

Figure 2: Visible satellite imagery at 2045 UTC 12 June 2002 with surface observations. Station models show wind barbs (one full barb representing approximately 5 m/s), and temperature and dewpoint temperature (°F) (Xue and Liu, 2008).

3. RESULTS

The control simulation initiated convection at 2025 UTC (Fig. 3). It appeared to resolve the HCRs in northwest Oklahoma approximately where the observed HCRs were located. In this location, there was evidence of ascending and descending branches of air existing in this location. Also, in theory, HCRs should have a decrease in water vapor mixing ratio in the descending branches, and increasing water vapor mixing ratio in the ascending branches (Weckwerth *et al.* 1996). This was shown in the model simulation as well. There was also evidence of cloud streets in the model that developed, which appeared to look like the typical "pearls on a string" that Kuettner (1959) used to describe some cloud streets.

The location of CI in the control simulation suggested that HCRs helped to focus CI, which agrees with the observations made in Weckwerth *et al.* (2008). However, the CI timing and location were different than that compared with the observed dataset. The location was ~50 km to the east of where the observed CI was, timing.

Overall, the simulation matched the correct CI mechanism, but it did not simulate the CI timing or location precisely. In any case, the control simulation
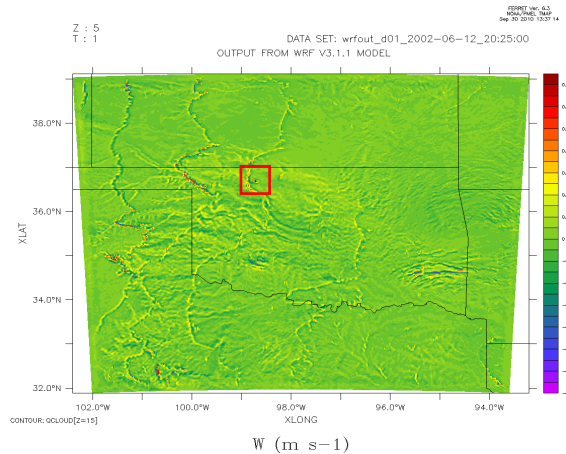

W (m s−1)

Figure 3: Vertical velocity with cloud water vapor mixing ratio contoured over it. In the red box is a black dot, which is the first indication that cumulus clouds developed above the LCL. This is how we determine when CI occurs. This is when CI occurred in the control simulation (2025 UTC).

will be used to compare the CI timing and location of the parameter perturbation simulations.

Fig. 4 shows the images of the moment of CI for the increase and decrease in potential temperature and water vapor mixing ratio. The boundary around the center of the domain shows the domain where the parameter perturbations were applied to throughout the depth of the boundary layer in the model simulation. Figs. 4a, 4b, 4c, and 4d are the decrease and increase in water vapor mixing ratio and the increase and decrease in potential temperature, respectively.

Table 2 shows a summary of when CI occurred for each case, including the control simulation. It is interesting to note that for the increase in potential temperature case, CI occurred after the control simulation, which went against our hypothesis for the increase in θ. However, we were correct in hypothesizing that an increase in water vapor mixing ratio would help CI occur sooner and a decrease in potential temperature and water vapor mixing ratio would force CI to occur later.

Since the parameter perturbations were performed through the depth of the boundary layer, we hypothesize that the reason CI occurred later for the increase in potential temperature case is because a warming throughout the depth of the boundary layer may make it warmer on the surface, but it also makes the boundary layer warmer aloft, which would assist in the strengthening of the capping inversion. It might be that the warming applied in the boundary layer depth of

the model helped to cap any potential convective development.

The only parameter perturbation that showed CI occurring before CI in our control simulation was the

in the observed data, and the model simulations. Hence, we conclude that the primary CI mechanism in these cases, even for the parameter perturbation simulations, is the HCRs.
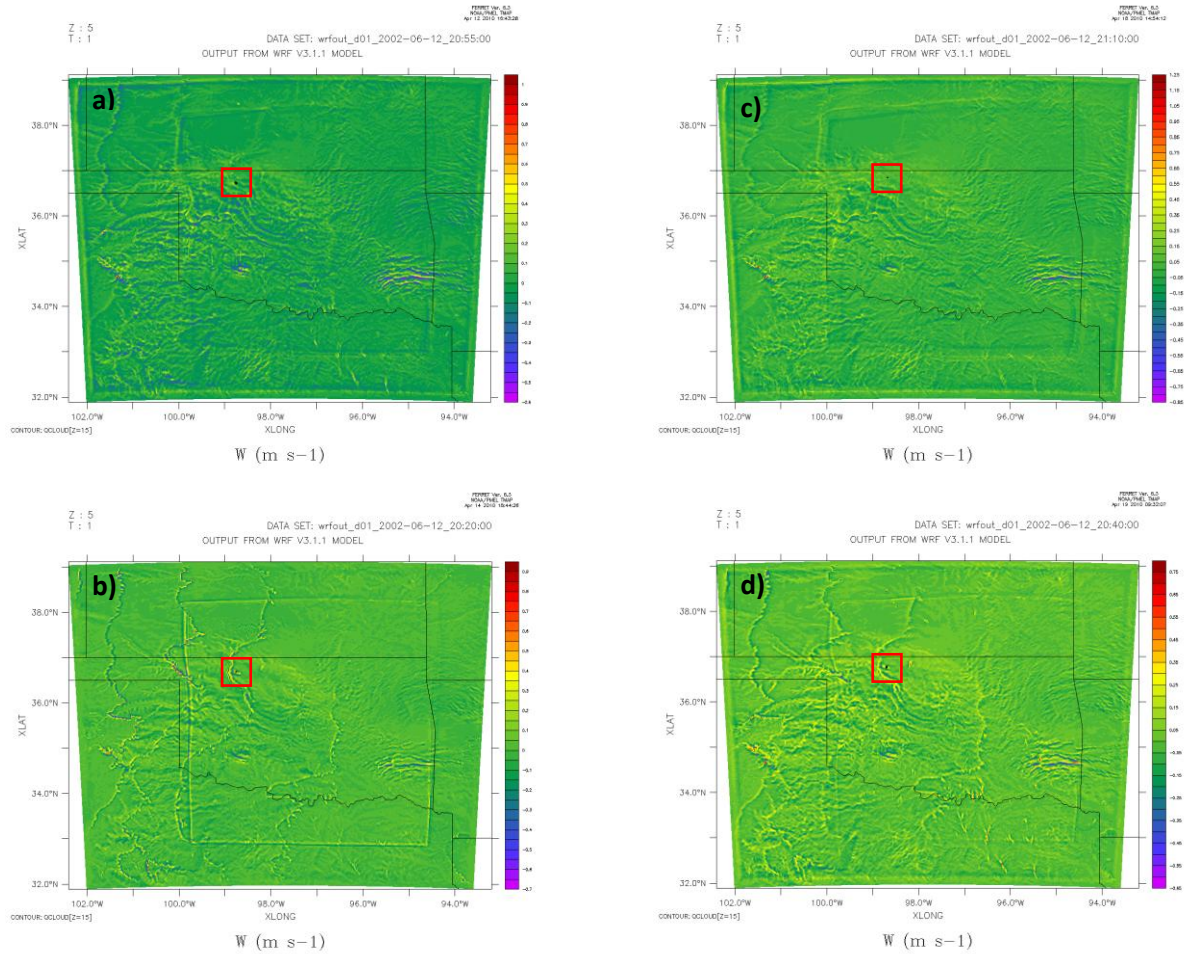

Figure 4: Images from the moment CI occurs in the parameter perturbation simulations. Figs. 4a-4d are the: decrease in water vapor mixing ratio, increase in water vapor mixing ratio, decrease in potential temperature, and the increase in potential temperature, with the timing of CI in the simulations are 2055, 2020, 2110, and 2040 UTC, respectively. Red boxes are again used to point out the location of CI.

increase in water vapor mixing ratio. This simulation was the most active, developing strong turbulence and very strong vertical velocities (with magnitudes into the double digits in the positive-z direction). It would make sense that perturbing water vapor mixing ratio would cause CI to occur sooner since on a skew-t ln-p diagram, the water vapor mixing ratio lines are steeper than the dry adiabatic lapse rate lines, which would imply that increasing the water vapor mixing ratio would help a lifted thermal reach its LFC quicker than increasing the potential temperature.

The location of CI appears to have occurred over the same location in each of the model simulations (approximately near the 36.8°N latitude by 98.7°W longitude intersection). This is the location of the HCRs

Simulation	CI Timing (UTC)
Control	2025
Water vapor mixing ratio increase	2020
Water vapor mixing ratio decrease	2055
Potential temperature increase	2040
Potential temperature decrease	2110

Table 2: Simulation type and CI timing for each simulation.

As the model simulations continued to run and simulate convection, the development of the subsequent convection then appeared to have developed primarily along the outflow boundary, which is where the highest amount of CAPE values were located. In the observed

data set, subsequent convection developed both along the outflow boundary and the dryline, located to the west of the HCRs. The convective development along the dryline did not occur in the model simulations, however. The reason is that it appears the dryline did not propagate eastward as quickly as it did in the observed data.

4. DISCUSSION

It is clear to see from the results section that HCRs were the most dominant CI mechanism for this case, and the WRF ARW simulations showed that additional subsequent convection was shown to be caused by the outflow boundary present in this case. The IHOP researchers on this day were stationed in the eastern section of the Oklahoma Panhandle, forecasting that CI would occur near the triple point (the mesolow), which is where the outflow boundary and the dryline intersect (Weckwerth *et al.* 2008). However, CI occurred east of the dryline and behind the outflow boundary, approximately 40 kilometers east of the IHOP observation region.

In our numerical modeling simulation, and in the observed data, it has been shown that HCRs helped initiate convection. Even though this is true, CAPE values were better along the outflow boundary. These sensitivity tests using the perturbation of the water vapor mixing ratio and potential temperature showed that the HCRs were indeed responsible for CI for this case, despite increasing/decreasing these parameters. However, would CI occur along the outflow boundary if additional convergence were added? This was also a question raised by Markowski *et al.* (2006), pondering as to why this CI did not occur along the outflow boundary despite better environmental conditions. They had hypothesized that a lack of moisture upwelling, and improper moisture transport by the outflow boundary doomed its chances of initiating convection. What if the outflow boundary created additional convergence that would help to transport additional moisture into the boundary layer? Would CI occur along the outflow boundary instead of the HCRs? These questions will be answered with another WRF ARW simulation. However, this new simulation will use a one-way nested domain inside the 2 km domain that was used for the parameter perturbation simulations. The nested grid domain will consist of a 500 meter grid resolution, 800×800 grid domain. The nested grid will have similar parameterization schemes activated as the 2 km simulation, expect the PBL scheme will be turned off. The simulation will still run through the 2000-2300 UTC time period to observe if a model with a finer resolution will resolve the HCRs, and how CI timing and location will change with this change in resolution.

This one-way nested simulation will also be used to test Markowski *et al.* (2006) hypotheses by introducing a cold pool ahead of the outflow boundary, which will create additional convergence to see if the outflow boundary will initiate convection before the HCRs do. If CI occurred along the outflow boundary before CI near the HCRs, this would confirm the validity of their hypotheses. The results of these simulations will be discussed at the SLS conference.

5. ACKNOWLEDGEMENTS

6. REFERENCES

Atkins, N. T., R. M. Wakimoto, and C. L. Ziegler, 1998: Observations of the Finescale Structure of a Dryline during VORTEX 95. *Mon. Wea. Rev.*, **126**, 525-550.

Byers, H. R., and R. R. Braham Jr., 1949: *The Thunderstorm*. U.S. Government Printing Office, 287 pp.

Faller, A. J., 1965: Large Eddies in the Atmospheric Boundary Layer and Their Possible Role in the Formation of Cloud Rows. *J. Atmos. Sci.,* **22**, 176-184.

Kuettner, J. P., 1959: The band structure of the atmospheric. *Tellus,* **11,** 267–294.

Lilly, D. K., 1966: On the Instability of Ekman Boundary Flow. *J. Atmos. Sci.,* **23**, 481-494.

Liu, H., and M. Xue, 2008: Prediction of convective initiation and storm evolution on 12 June 2002 during IHOP_2002. Part I: Control simulation and sensitivity experiments. *Mon. Wea. Rev.,* **136,** 2261–2282.

Markowski, P., C. Hannon, and E. Rasmussen, 2006: Observations of convection initiation "failure" from the 12 June 2002 IHOP deployment. *Mon. Wea. Rev.*, **134**, 375–405.

Schaefer, J. T., 1986: Severe Thunderstorm Forecasting: A Historical Perspective. *Wea. Forecasting,* **1**, 164-189.

Skamarock, W. C., J. B. Klemp, and J. Dudhia: Prototypes for the WRF (Weather Research and Forecasting) model. *Preprints, Ninth Conf. on*

Mesoscale Processes, Fort Lauderdale, FL, Amer. Meteor. Soc., J11—J15, 2001.

Stull, R. B., 1988: *An Introduction to Boundary Layer Meteorology.* Springer Science and Business Media B.V., 670 pp.

Weckwerth, T. M., J. W. Wilson, and R. M. Wakimoto, 1996: Thermodynamic variability within the convective boundary layer due to horizontal convective rolls. *Mon. Wea. Rev.,* **124,** 769–784.

——, J. W. Wilson, R.M. Wakimoto, and N. A. Crook, 1997: Horizontal convective rolls: Determining the environmental conditions supporting their existence and characteristics. *Mon. Wea. Rev.,* **125,** 505–526.

——, Coauthors, 2004: An overview of the International H_2O Project (IHOP_2002) and some preliminary highlights. *Bull. Amer. Meteor. Soc.*, **85**, 253–277.

——, H. V. Murphey, C. Flamant, J. Goldstein, C. R. Pettet, 2008: An Observational Study of Convection Initiation on 12 June 2002 during IHOP_2002. *Mon. Wea. Rev.*, **136**, 2283-2304.

——, and R. M. Wakimoto, 1992: The initiation and organization of convective cells atop a cold-air outflow boundary. *Mon. Wea. Rev.,* **120,** 2169–2187.

Wilhelmson, R. B., and C. Chen, 1982: A Simulation of the Development of Successive Cells Along a Cold Outflow Boundary. *J. Atmos. Sci.,* **39**, 1466-1483.

Wilson, J. W., and R. D. Roberts, 2006: Summary of convective storm initiation and evolution during IHOP: Observational and modeling perspective. *Mon. Wea. Rev.,* **134,** 23–47.

Ziegler, C. L., T. J. Lee, R. A. Pielke, Sr., 1997: Convective Initiation at the Dryline: A Modeling Study. *Mon. Wea. Rev.*, **125**, 1001-1026.